



1

2 **Providing a non-deterministic representation of spatial variability of**  
3 **precipitation in the Everest region.**

4 Judith Eeckman<sup>a</sup>, Pierre Chevallier<sup>a</sup>, Aaron Boone<sup>b</sup>, Luc Neppel<sup>a</sup>, Anneke De  
5 Rouw<sup>c</sup>, Francois Delclaux<sup>a</sup>, Devesh Koirala<sup>d</sup>

6 <sup>a</sup>Laboratoire HydroSciences (CNRS, IRD, Universite de Montpellier) CC 57 - Universite de  
7 Montpellier 163, rue Auguste Broussonnet 34090 Montpellier, France;

8 <sup>b</sup>CNRM UMR 3589, Meteo-France/CNRS, Toulouse, France;

9 <sup>c</sup>Institut de Recherche pour le Developpement, Universite Pierre et Marie Curie, 4 place  
10 Jussieu, 75252 Paris cedex 5, France;

11 <sup>d</sup>Nepal Academy of Science and Technology GPO box: 3323 Khumaltar, Lalitpur, Nepal

12

13

14 **ABSTRACT**

15 This paper provides a new representation of the effect of altitude on precipitation  
16 that represent spatial and temporal variability of precipitation in the Everest re-  
17 gion. Exclusive observation data are used to infer a piecewise linear function for  
18 the relation between altitude and precipitation and significant seasonal variations  
19 are highlighted. An original ensemble approach is applied to provide non determin-  
20 istic water budgets for middle and high mountain catchments. Physical processes  
21 at the soil-atmosphere interface are represented through the ISBA surface scheme.  
22 Uncertainties associated with the model parametrization are limited by the inte-  
23 gration of in-situ measurements of soils and vegetation properties. Uncertainties  
24 associated with representation of the orographic effect are shown to account for up  
25 to 16% of annual total precipitation. Annual evapotranspiration is shown to rep-  
26 resent  $26\% \pm 1\%$  of annual total precipitation for the mid-altitude catchment and  
27  $34\% \pm 3\%$  for the high-altitude catchment. Snow fall contribution is shown to be  
28 neglectible for the mid-altitude catchment and it represents up to  $44\% \pm 8\%$  of total  
29 precipitation for the high-altitude catchment. These simulations at the local scale  
30 enhance current knowledge of the spatial variability of hydro-climatic processes in  
31 high- and mid-altitude mountain environments.

32 **KEYWORDS**

33 Central Himalayas; precipitation; uncertainty analysis; ISBA surface scheme

34 **1. Introduction**

35 The central part of the Hindu Kush Himalaya region presents tremendous heterogene-  
36 ity, in particular in terms of topography and climatology. The terrain ranges from  
37 the agricultural plain of Terai to the highest peaks of the world, including Mount  
38 Everest, over a south-north transect about 150km long (FIGURE 1).

39

40 Two main climatic processes at the synoptic scale are distinguished in the Central  
41 Himalayas (Barros *et al.* 2000, Kansakar *et al.* 2004). First, the Indian Monsoon is

---

Judith Eeckman [judith.eeckman-poivilliers@univ-montp2.fr](mailto:judith.eeckman-poivilliers@univ-montp2.fr)



42 formed when moist air arriving from Bay of Bengal is forced to rise and condense  
43 on the Himalayan barrier. Dhar and Rakhecha (1981) and Bookhagen and Burbank  
44 (2010) assessed that about 80% of annual precipitation over the Central Himalayas  
45 occurs between June and September. However, the timing and intensity of this  
46 summer monsoon is being reconsidered in the context of climate change (Bharati  
47 *et al.* 2016). The second main climatic process is a west flux that gets stuck in  
48 adequately oriented valleys, and occurs between January and March. Regarding high  
49 altitudes ( $> 3000$  m), this winter precipitation can occur exclusively in solid form  
50 and can account for up to 40% of annual precipitation (Lang and Barros 2004) with  
51 considerable spatial and temporal variation.

52  
53 At a large spatio temporal scale, precipitation patterns over the Himalayan  
54 range are recognized to be strongly dependent on topography (Anders *et al.* 2006,  
55 Bookhagen and Burbank 2006, Shrestha *et al.* 2012). The main thermodynamic  
56 process is an adiabatic expansion when air masses rise, but, at very high altitudes  
57 ( $> 4000$  m), the reduction of available moisture is a concurrent process. Altitudinal  
58 thresholds of precipitation can then be discerned (Alpert 1986, Roe 2005). However,  
59 this representation of orographic precipitation has to be modulated considering the  
60 influence of such a protruding relief (Barros *et al.* 2004).

61  
62 Products for precipitation estimation currently available in this area, e.g. the  
63 APHRODITE interpolation product (Yatagai *et al.* 2012) and the TRMM remote  
64 product (Bookhagen and Burbank 2006), do not represent spatial and temporal vari-  
65 ability of orographic effects at a resolution smaller than 10 km (Gonga-Saholiariliva  
66 *et al.* 2016). Consequently, substantial uncertainty remains in water budgets simulated  
67 for this region, as highlighted by Savéan *et al.* (2015). In this context, ground-based  
68 measurements condensed in small areas have been shown to enhance the characteri-  
69 zation of local variability of orographic processes (Andermann *et al.* 2011, Pellicciotti  
70 *et al.* 2012, Immerzeel *et al.* 2014). However, even if the Everest region is one of the  
71 most closely monitored areas of the Himalayan range, valuable observations remain  
72 scarce. In particular, the relation between altitude and precipitation is still poorly  
73 documented.

74  
75 The objective of this paper is to provide a representation of the effect of altitude  
76 on precipitation that represent spatial and temporal variability of precipitation in  
77 the Everest region. The parameters controlling the shape of the altitudinal factor  
78 are constrained through an original sensitivity analysis step. Uncertainties associated  
79 with variables simulated through the ISBA surface scheme (Noilhan and Planton  
80 1989) are quantified.

81  
82 The first section of the paper presents the observation network and recorded data.  
83 The second section describes the model chosen to represent orographic precipitation,  
84 including computed altitude lapse rates for air temperature and precipitation. The  
85 method for statistical analysis through hydrological modeling is also described. The  
86 third section presents and discusses the results of sensitivity analysis and uncertainty  
87 analysis.

88 **2. Data and associated uncertainties**89 **2.1. Meteorological station transect**

90 An observation network of ten stations (FIGURE 1) records hourly precipitation  
91 (P) and air temperature (T) since 2010 and 2014. The stations are equipped with  
92 classical rain gauges and HOBO® sensors for temperature. The stations are located  
93 to depict altitudinal profile of P and T over 1) the main river valley (Dudh Koshi  
94 valley), oriented south-north; 2) the Kharikhola tributary river, oriented east-west.

95  
96 To reduce under-catching of solid precipitation, two Geonors® were installed at  
97 4218 m and 5035 m in 2013. Measurements at Geonor® instrumentation allow to  
98 correct the effect of wind and the loss of snowflakes. Records from four other stations  
99 administrated by the EVK2-CNR association are also available. Total precipitation, air  
100 temperature, atmospheric pressure (AP), relative humidity (RH), wind speed (WS),  
101 short-wave radiation (direct and diffuse) (SW) and long-wave radiation (LW) have  
102 been recorded at the hourly time step since 2000 at Pyramid station (5035 m.a.s.l.).  
103 Overall, these ten stations cover an altitude range from 2078 m to 5035 m a.s.l.,  
104 comprising a highly dense observation network, compared to the scarcity of ground-  
105 based data in this type of environment.

**Table 1.** Overview of the observation network used in this study. Air temperature (T), precipitation (P) atmospheric pressure (AP), relative humidity (RH), wind speed (WS), short- and long-wave radiation (SW, LW) are recorded at the hourly time scale. The Geonor® at the Pyramid and Pheriche stations record total precipitation  $P_{GEO}$  at the hourly time scale. The two hydrometric stations at Kharikhola and Pangboche record water level since 2014.

ID	Station	ALT m.a.s.l.	LAT	LON	Period		Measured variable
KHA	Kharikhola	2078	27.60292	86.70311	2014-05-03	2015-10-28	P,T
MER	Mera School	2561	27.60000	86.72269	2014-05-02	2015-10-28	P,T
BAL	Bhalukhop	2575	27.60097	86.74017	2014-05-03	2015-10-28	P,T
PHA	Phakding	2619	27.74661	86.71300	2010-04-07	2016-05-16	P,T
LUK	Lukla	2860	27.69694	86.72270	2002-11-02	2016-01-01	P,T
PAR	Paramdingma	2869	27.58492	86.73956	2014-05-03	2015-10-28	P,T
TCM	Pangom	3022	27.58803	86.74828	2014-05-03	2015-10-28	P,T
NAM	Namche	3570	27.80250	86.71445	2001-10-27	2016-01-01	P,T
PAN	Pangboche	3976	27.85722	86.79417	2010-10-29	2016-05-08	P,T
PHE	Pheriche	4218	27.89528	86.81889	2001-10-25	2016-01-01	T
PYR	Pyramid	5035	27.95917	86.81333	2000-10-01	2016-01-01	$P_{GEO}$
					2012-12-06	2016-05-16	T,AP,RH,WS, LW,SW
					2016-04-26	2016-04-26	$P_{GEO}$
668.7	Kharikhola	1985	27.60660	86.71847	2014-05-03	2016-05-20	Water level
668.03	Pangboche	3976	27.85858	86.79253	2014-05-17	2016-05-09	Water level

106 Annual means for temperature and precipitation measured at these stations are  
107 presented are presented TABLE 2 for the two hydrological years 2014-2015 and  
108 2015-2016. These time series present up to 61% missing values. For stations LUK,  
109 NAM, PHA, PAN, PHE and PYR, where relatively long time series are available,  
110 gaps were filled with the interannual hourly mean for each variable. For the other  
111 stations, gaps were filled with values at the closest station, weighted by the ratio of  
112 mean values over the common periods. Time series from 2013-01-01 to 2016-04-30  
113 were then reconstructed from these observations.

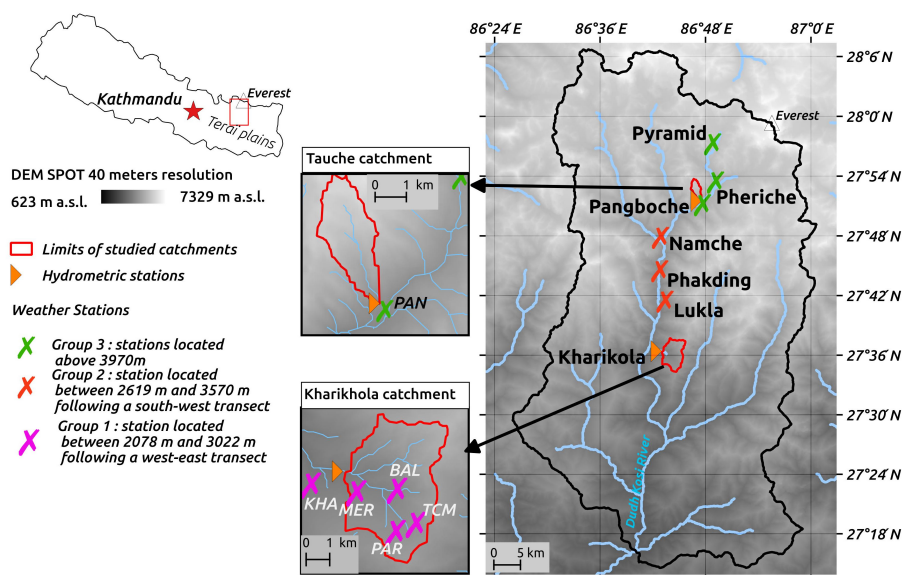


**Figure 1.** Map of the monitored area: the Dudh Koshi River basin at the Rabuwabazar station, managed by the Department of Hydrology and Meteorology, Nepal Government (station coordinates:  $27^{\circ}16'09''N$ ,  $86^{\circ}40'03''E$ , station elevation: 462 m a.s.l., basin area: 3712 km<sup>2</sup>). The Tauche and Kharikhola subcatchments are defined by the corresponding limnietric stations.

114

115 Two seasons are defined based on these observations and knowledge of the clima-  
 116 tology of the Central Himalayas: 1) the monsoon season, from April to September,  
 117 including the early monsoon, whose influence seems to be increasing with the recent  
 118 climate change (Bharati *et al.* 2014); 2) the winter season, dominated by westerly  
 119 entrances with a substantial spatiotemporal variability.

120

121 Local measurements are necessarily biased by aleatory errors (according to Beven  
 122 (2015) uncertainty classification). In particular, snowfall is usually undercaught by  
 123 instrumentation (Sevruk *et al.* 2009). However, since this study focuses most particu-  
 124 larly on uncertainty associated with spatialization of local measurements, aleatory  
 125 errors in measurements will not be considered here.

## 126 2.2. Discharge measurement stations and associated hydrological 127 catchments

128 Two hydrometric stations were equipped with Campell® hydrometric sensors and en-  
 129 compass two sub-basins: Kharikhola catchment (18.2km<sup>2</sup>) covers altitudes from 1900  
 130 m to 4450 m (mid-altitude mountain catchment) and Tauche catchment (4.65km<sup>2</sup>)  
 131 altitudes range from 3700 m to 6400 m (high-altitude mountain catchment). Water  
 132 level time series are available from March 2014 to March 2015, with 16.5% and 0%  
 133 data gaps, respectively (TABLE 3). Uncertainty on discharge is usually considered to  
 134 account for less than 15% of discharge (Lang *et al.* 2006).



135

136

Recession times are computed on available recession periods using the `lfstat` R library (Koffler and Laaha 2013) with both the recession curves method (World Meteorological Organization 2008) and the base flow index method (Chapman 1999). We found recession times for Kharikhola and Tauche catchment of respectively around 70 days and around 67 days. Consequently, we consider that there is no interannual storage in either of the two catchments. This hypothesis can be modulated if a contribution of deep groundwater is considered (Andermann *et al.* 2011). Since these two catchments have null (Kharikhola) or neglectible (Tauche) glacier contribution, we hypothesized that the only entrance for water budgets in these catchments is total precipitation. In this study we used these two catchments as samples to assess generated precipitation fields against observed discharge at the local scale. The hydrological year is considered to start on 1 April, as decided by the Department of Hydrology and Meteorology of the Nepalese Government and generally considered (Nepal *et al.* 2014, Savéan *et al.* 2015).

137

138

139

140

141

142

143

144

145

146

147

148

149

**Table 2.** Overview of measurements at meteorological stations used in this study over the hydrological years 2014-2015 and 2015-2016.  $\bar{T}$ ,  $\bar{P}$  stand for, respectively, annual mean temperature and annual total precipitation.  $\bar{T}$ ,  $\bar{P}$  are computed on time series completed with either a weighted value at the closest station when available, or their respective interannual mean.

Station	2014-2015				2015-2016			
	Temperature		Precipitation		Temperature		Precipitation	
	$\bar{T}$ °C	Gaps	$\bar{P}$ mm	Gaps	$\bar{T}$ °C	Gaps	$\bar{P}$ mm	Gaps
KHA	13.96	0.1%	2453	34.5%	15.50	100%	1752	100%
MER	13.44	12.4%	3241	12.2%	14.83	100%	2278	100%
BAL	9.92	15.1%	3679	34.4%	10.48	0.0%	2628	0.0%
PHA	9.26	41.9%	1664	0.0%	9.16	0.0%	1226	0.0%
LUK	10.18	54.5%	2278	41.8%	10.19	40%	2278	0.2%
PAR	7.98	20%	3592	19.8%	7.84	100%	2540	100%
TCM	7.07	21.1%	3592	20.8%	6.90	100%	2628	100%
NAM	5.09	19.9%	964	0.1%	5.17	57.9%	788	0.1%
PAN	3.81	0.2%	876	0.0%	4.20	0.0%	526	0.0%
PHE	0.80	61%	701	0.0%	0.84	8.6%	526	0.0%
PYR	-2.71	18.6%	701	0.0%	-2.30	9.3%	438	0.0%

**Table 3.** Overview of measurements at hydrological stations used in this study over the hydrological years 2014-2015 and 2015-2016.  $\bar{Q}$  stands for annual discharge.  $\bar{Q}$  for the Kharikhola station in 2014-2015 is completed with the interannual mean.

Station	2014-2015		2015-2016	
	$\bar{Q}$	Gaps	$\bar{Q}$	Gaps
	mm		mm	
Kharikhola	2341	34.0%	1746	0.0%
Pangboche	416	0.0%	499	0.0%



### 150 3. Spatialization methods for temperature and precipitation

#### 151 3.1. Temperature

152 In mountainous areas, temperature and altitude generally correlate well linearly, con-  
153 sidering a large time scale (Valéry *et al.* 2010, Gottardi *et al.* 2012). In the majority of  
154 studies based on field observations, air temperature values are extrapolated using the  
155 inverse distance weighting method (IDW) (Andermann *et al.* 2012, Immerzeel *et al.*  
156 2012, Nepal *et al.* 2014). An altitude lapse rate  $\theta$  (in  $^{\circ}C.km^{-1}$ ) is also used to take  
157 altitude into account for hourly temperature computation at any point M of the mesh  
158 extrapolated by IDW (EQUATION 1).

$$T(M) = \frac{\sum_{S_i} d^{-1}(M, S_i) \cdot (T(S_i) + \theta \cdot (z_M - z_i))}{\sum_{S_i} d^{-1}(M, S_i)} \quad (1)$$

159 where  $T$  is the hourly temperature,  $S_i$  the  $i$ th station of the observation network,  
160  $z_i$  the altitude of station  $S_i$ ,  $z_M$  altitude of grid point M and  $d^{-1}$  is the inverse of  
161 distance in latitude and longitude.

162  
163 In the Himalayas, seasonal (Nepal *et al.* 2014, Ragetti *et al.* 2015) or constant  
164 (Pokhrel *et al.* 2014) altitudinal lapse rates (LR) are used for temperature. FIGURE  
165 2 presents seasonal LR computed from temperature time series at the 10 stations  
166 described in section 2.1. The linearity is particularly satisfying for both seasons, even  
167 if stations follow differently oriented transects (W-E or N-S orientation). Computed  
168 LR for both seasons are very close to values proposed by Immerzeel *et al.* (2014),  
169 Heynen *et al.* (2016) (Langtang catchment, 585  $km^2$ , elevation ranging from 1406  
170 m.a.s.l. to 7234 m.a.s.l.) and Salerno *et al.* (2015) (Koshi basin, 58100  $km^2$ , from 77  
171 m.a.s.l. to 8848 m.a.s.l.). Consequently, these values for seasonal LR will be used in  
172 this study. Uncertainties associated with temperature interpolation will therefore be  
173 neglected, because they have minor impact on modelling compared to uncertainties  
174 on precipitation.

#### 175 3.2. Precipitation

##### 176 3.2.1. Model of orographic precipitation

177 The complexity of precipitation spatialization methods has been commented by Bar-  
178 ros and Lettenmaier (1993). When orographic effects are not well understood, complex  
179 approaches do not necessarily reproduce local measurements efficiently (Bénichou and  
180 Le Breton 1987, Frei and Schär 1998, Daly *et al.* 2002). In the Central Himalayas, var-  
181 ious hydrologic and glaciological studies are based on observation networks to produce  
182 a precipitation grid. They use either observed altitude lapse rates, e.g., in the Lang-  
183 tang range, (Immerzeel *et al.* 2012, Ragetti *et al.* 2015) and in the Dudh Koshi River  
184 basin, (Nepal *et al.* 2014), or geostatistical methods (Gonga-Saholiariliva *et al.* 2016)  
185 (Koshi catchment). Nevertheless, the IDW method is a simple, widely used method  
186 to spatialize precipitation. In the French Alps, Valéry *et al.* (2010) combine the IDW  
187 method with a multiplicative altitudinal factor. Precipitation at any point M of the  
188 mesh extrapolated by the IDW is given by EQUATION 2.

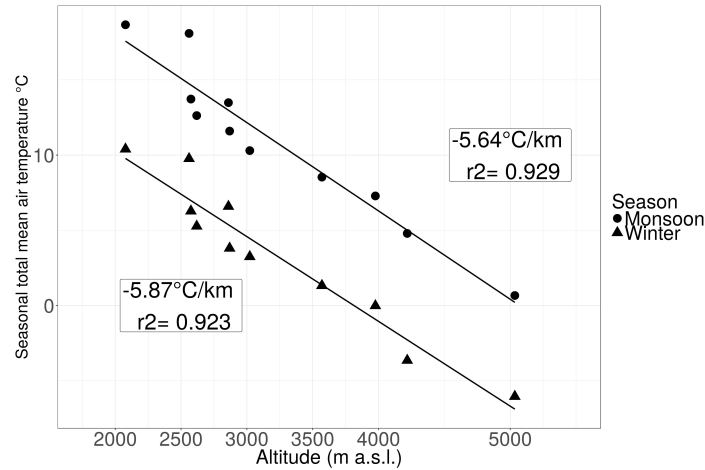


**Figure 2.** Linear regression for measured seasonal temperatures for the winter and monsoon seasons. Points (circles or triangles) are the seasonal means at each monitored station. Altitude lapse rates are displayed for each season in  $^{\circ}C.km^{-1}$ .

$$P(M) = \frac{\sum_{S_i} d^{-1}(M, S_i) \cdot (P(S_i) \cdot \exp(\beta(z_M - z_i)))}{\sum_{S_i} d^{-1}(M, S_i)} \quad (2)$$

189 In EQUATION 2, the altitude effect is represented through the introduction of the  
 190 altitudinal factor  $\beta$ , defined by Valéry *et al.* (2010) as the slope of the linear regression  
 191 between the altitude of stations (in m.a.s.l.) and the logarithm of seasonal volume of  
 192 total precipitation expressed in millimeters.

### 193 3.2.2. Observed relation between altitude and seasonal precipitation

194 Several studies based on observations (Dhar and Rakhecha 1981, Barros *et al.*  
 195 2000, Bookhagen and Burbank 2006, Immerzeel *et al.* 2014, Salerno *et al.* 2015),  
 196 or theoretical approaches (Burns 1953, Alpert 1986) observed that precipitation in  
 197 the Himalayan range generally presents a multimodal distribution along elevation.  
 198 Precipitation is considered to increase with altitude until a first altitudinal threshold  
 199 located between 1800 m and 2500 m, depending on the study, and to decrease above  
 200 2500m. Moreover, the linear correlation of precipitation with altitude is reported to  
 201 be weak for measurements above 4000 m (Salerno *et al.* 2015). The decreasing of  
 202 precipitation with altitude are characterized through various fonctions (Dhar and  
 203 Rakhecha 1981, Bookhagen and Burbank 2006, Salerno *et al.* 2015). Nevertheless,  
 204 the hypothesis of linearity of precipitation (P) with altitude (z) is often made, with  
 205 a constant (Nepal *et al.* 2014) or time-dependent lapse rate (Immerzeel *et al.* 2014).  
 206 Gottardi *et al.* (2012) noted that, in mountainous areas, the hypothesis of a linear  
 207 relation between P and z is only acceptable over a small spatial extension and for  
 208 homogeneous weather types. Consequently, we considered altitude lapse rates for



209 precipitation at the seasonal time scale, and we analyzed the spatial variability of the  
 210 relation between P and z.

211  
 212 For this purpose, we chose to regroup the stations into three groups (see FIGURE  
 213 1): 1) stations with elevation ranging from 2078 m to 3022 m, following a west-east  
 214 transect (Group 1) ; 2) stations with elevation ranging from 2619 m to 3570 m  
 215 following a south-west transect (Group 2); and 3) stations with elevation above 3970  
 216 m (Group 3). FIGURE 3 shows that 1) for Group 1, observed seasonal volumes of  
 217 precipitation increase globally with altitude at a rate lower than  $0.1km^{-1}$ ; 2) for  
 218 Group 2, seasonal volumes decrease at a rate around  $-0.3km^{-1}$  ; 3) for Group 3,  
 219 seasonal volumes decrease at a rate lower than  $0.2km^{-1}$ , with a poor linear trend.

220  
 221 The overlapping of altitude ranges between Group 1 and Group 2 highlights that  
 222 the relation between precipitation and altitude strongly depends on terrain orientation.  
 223 The difference in seasonal volumes at the BAL (2575 m a.s.l., 3471 mm/year)  
 224 and MER stations (2561 m a.s.l., 2245 mm/year) (GROUP 1) also result from site  
 225 effects on precipitation. In summary,  $\beta$  values inferred from local observations mainly  
 226 express local variability and are not sufficient to establish any explicit relation between  
 227 precipitation and altitude at the catchment scale. However, for operational purposes,  
 228 the  $\beta$  factor can be simplified as a multi-modal function of altitude within the Dudh  
 229 Koshi catchment. Optimum values that optimally fit local variability were then investi-  
 230 gated through a sensitivity and uncertainty analysis. The  $\beta$  factor is represented as  
 231 a piecewise linear function of altitude using two altitudinal thresholds  $z_1$  and  $z_2$  and  
 232 three altitude lapse rates  $\beta_1$ ,  $\beta_2$  and  $\beta_3$  (EQUATION 3).

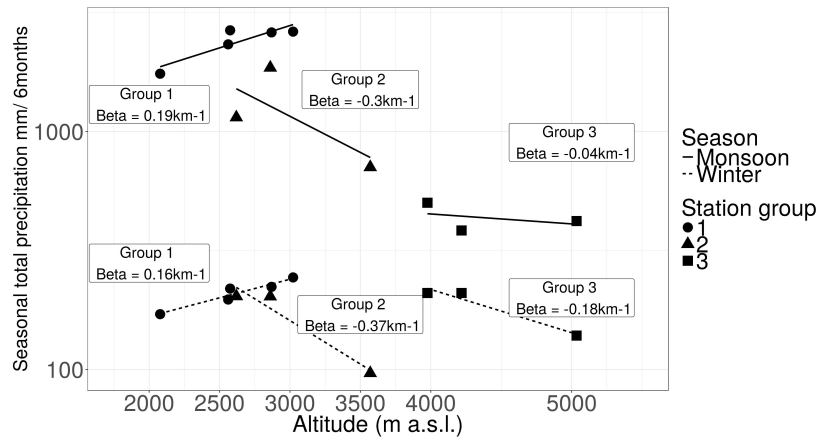


**Figure 3.** Piecewise relation between altitude and the logarithm of observed seasonal volumes of total precipitation, separated by season and station group. Seasonal values for  $\beta$  ( $km^{-1}$ ) are computed from observed precipitation for each of the three station groups.

$$\beta(z) = \begin{cases} \beta_1 > 0 & \text{if } z \leq z_1 \\ \beta_2 < 0 & \text{if } z_1 < z \leq z_2 \\ \beta_3 \sim 0 & \text{if } z > z_2 \end{cases} \quad (3)$$



233 Since no deterministic value can be ensured for the five parameters controlling the  
234 shape of EQUATION 3, an ensemble approach was applied (see Section 4) to estimate  
235 parameter sets at the scale of the entire Dudh Koshi River basin that are optimally  
236 suitable for both Tauche and Kharikhola catchments.

## 237 4. Sensitivity and uncertainties analysis method

### 238 4.1. Overall strategy

239 Saltelli *et al.* (2006) distinguishes sensitivity analysis (SA), which does not provide a  
240 measurement of error, and uncertainties analysis (UA), which computes a likelihood  
241 function according to reference data. SA is run before UA as a diagnostic tool, in  
242 particular to reduce variation intervals for parameters and therefore save computation  
243 time.

244  
245 The algorithm chosen for SA was the Regional Sensitivity Analysis (RSA) (Spear  
246 and Hornberger 1980) method. The RSA method is based on the separation of the  
247 parameter space into (at least) two groups: behavioral or nonbehavioral parameter  
248 sets. A behavioral parameter set is a set that respects conditions (maximum or mini-  
249 mum thresholds) on the output of the orographic precipitation model. Thresholds will  
250 be defined for solid and total precipitation in the Results section. The analysis is per-  
251 formed using the R version of the SAFE(R) toolbox, developed by Pianosi *et al.* (2015).

252  
253 SA and UA are set up as follows (Beven 2010):

- 254 (1) First, the parameter space is sampled, according to a given sampling distribution.  
255 For each parameter set, hourly precipitation fields are computed at the 1-km res-  
256 olution using EQUATION 2 for both the Tauche and Kharikhola catchments.  
257 Since physical processes condition the relation between altitude and precipita-  
258 tion strongly differ between the two seasons, we chose to distinguish altitude  
259 correction for the winter and monsoon seasons. Behavioral parameter sets were  
260 then selected for each of the two seasons.
- 261 (2) Then, for each behavioral precipitation field, the ISBA surface scheme, described  
262 in the next section, was run separately on Kharikhola and Tauche catchments.  
263 The objective function was computed as the difference between simulated and  
264 observed annual discharge at the outlet of each catchment. Parameter sets that  
265 lead to acceptable discharge regarding observed discharge for the two catchments  
266 are finally selected.

### 267 4.2. Hydrological modeling at the local scale

#### 268 4.2.1. The ISBA surface scheme

269 We considered that there was no interannual storage in either of the two subcatch-  
270 ments studied, i.e., the variation of the groundwater content was considered null from  
271 one hydrological year to the other. Consequently, annual simulated discharges were  
272 computed as the sum over all grid cells and all time steps, of simulated surface flow  
273 and simulated subsurface flow. The question of calibration of flow routing in the  
274 catchment was thus avoided.

275



276 The ISBA surface scheme (Noilhan and Planton 1989, Noilhan and Mahfouf 1996)  
277 simulates interactions between the soil, vegetation and the atmosphere on a sub-hourly  
278 time step (SVAT model). The multi-layer version of ISBA (ISBA-DIF) uses a diffusive  
279 approach (Boone *et al.* 2000, Decharme *et al.* 2011): surface and soil water fluxes are  
280 propagated from the surface through the soil column. Transport equations for mass  
281 and energy are solving using a multilayer vertical discretization of the soil. The explicit  
282 snow scheme in ISBA (ISBA-ES) Boone and Etchevers (2001) uses a three-layer  
283 vertical discretization of snow pack and provides a mass and energy balance for each  
284 layer (Boone and Etchevers 2001). Snow-melt and snow sublimation are taken into  
285 account in balance equations. The separation between runoff over saturated areas  
286 (Dunne runoff), infiltration excess runoff (Horton runoff) and infiltration is controlled by the Variable Infiltration Capacity Scheme (VIC) (Dümenil and Todini 1992).  
287

288  
289 The precipitation phase was estimated depending on hourly air temperature readings.  
290 Mixed phases occurred for temperatures between 0°C and 2°C, following a linear  
291 relation. Other input variables required for ISBA (atmospheric pressure, relative  
292 humidity, wind speed, short- and long-wave radiations) are interpolated from measurements at Pyramid station as functions of altitude, using the method proposed by  
293 Cosgrove *et al.* (2003). Short wave radiation and wind speed are not spatially interpolated and are considered to be equals to the measurements at Pyramid station for  
294  
295  
296 the two catchments.

#### 297 4.2.2. Parametrization of surfaces

298 Several products provide parameter sets for physical properties of surfaces at the  
299 global scale (Hagemann 2002, Masson *et al.* 2003, Arino *et al.* 2012). However,  
300 these products are not accurate enough at the resolution required for this study.  
301 The most recent analysis (Bharati *et al.* 2014, Ragettli *et al.* 2015) exclusively  
302 used knowledge garnered from the literature. To detail the approach, in this study  
303 the parametrization was based on in situ measurements. A classification into nine  
304 classes of soil/vegetation entities was defined based on Sentinel2 images at a 10-m  
305 resolution (Drusch *et al.* 2012), using a supervised classification tool of the QGIS  
306 Semi-Automatic Classification Plugin (Congedo 2015).  
307

308 In and around the two catchments, 24 reference sites were sampled during field  
309 missions. Data collection included soil texture, soil depth, root depth, determined by  
310 augering to a maximum depth of 1.2m. Vegetation height, structure and dominant  
311 plant species were also determined. The results were classified into nine surface types.  
312 The nine classes and their respective fractions in Kharikhola and Tauche catchments  
313 are presented TABLE 4.  
314

315 Analysis of soil samples showed that soils were mostly sandy (~ 70%), with a small  
316 proportion of clay (~ 1%). Soil depths varied from very thin (~ 30 cm) at high altitudes to 1.2 m for flat cultivated areas. Forest areas were separated into three classes: dry forests were characterized by high slopes and shallow soils; wet forests presented deep silty soils (1 m), with high trees (7 m). Intermediate forests had moderate slopes and relatively deep, sandy soils. Crop areas presented different soil depths depending on their average slope. In addition, values for unmeasured variables (LAI, soil and vegetation albedos, surface emissivity, surface roughness) were taken from the ECO-CLIMAP classification (Masson *et al.* 2003) for ecosystems representative of the study  
322  
323



324 area. ECOCLIMAP provides the annual cycle of dynamic vegetation variables, based  
 325 both on a surface properties classification (Hagemann 2002) and on a global climate  
 326 map (Koeppel and De Long 1958).

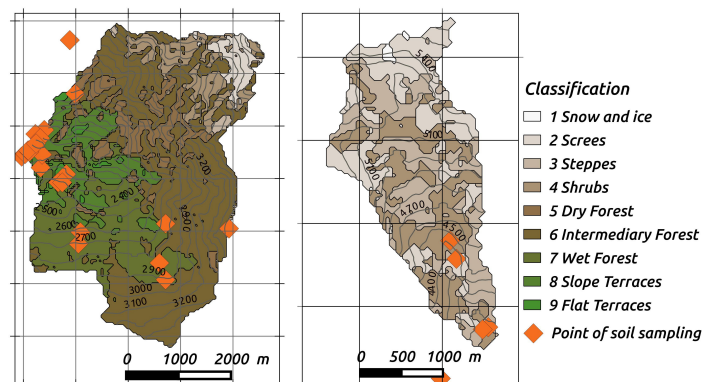


**Figure 4.** Classification of surfaces defined for the two Kharikhola and Tauche subcatchments, established using the supervised classification tool of the QGIS Semi-Automatic Classification Plugin (Congedo 2015), based on Sentinel2 images at a 10-m resolution (Drusch *et al.* 2012). In situ sample points were used to describe the soil and vegetation characteristics of each class.

**Table 4.** Soil and vegetation characteristics of the nine classes defined in Kharikhola and Tauche catchments, respectively. % KK and % Tauche are the fraction of each class on Kharikhola and Tauche catchments. Sand and clay fractions (% Sand and % Clay, respectively), soil depth (SD), root depth (RD) and tree height (TH) are defined based on in situ measurements. The dynamic variables (e.g. the fraction of vegetation and Leaf Area Index) were found in the ECOCLIMAP classification (Masson *et al.* 2003) for representative ecosystems.

ID	Class	% KK	% Tauche	% Sand	% Clay	TH m	SD m	RD m	Ecoclimap Cover
1	Snow and ice	-	0.7%	0.00	0.00	0.0	0.00	0.00	6
2	Screes	3.1%	31.2%	0.00	0.00	0.0	0.00	0.00	5
3	Steppe	0.6%	33.7%	81.41	1.70	0.0	0.10	0.10	123
4	Shrubs	7.4%	34.4%	70.60	1.55	0.0	0.35	0.27	86
5	Dry Forest	9.7%	-	72.86	1.00	12.0	0.20	0.20	27
6	Intermediary Forest	45.7%	-	84.97	1.01	27.5	0.42	0.40	27
7	Wet Forest	20.6%	-	70.12	1.00	6.8	1.04	0.50	27
8	Slope terraces	11.2%	-	70.89	1.38	5.6	0.56	0.26	171
9	Flat terraces	1.4%	-	67.01	1.69	2.5	1.267	0.20	171

## 327 5. Results and discussion

### 328 5.1. Regional sensitivity analysis

329 The parameter space was sampled using the All at a time (AAT) sampling algorithm  
 330 from the SAFE(R) toolbox (Pianosi *et al.* 2015). Since no particular information was  
 331 available on prior distribution and interaction for the five parameters, uniform distri-  
 332 butions were considered. The initial ranges for  $\beta_1$ ,  $\beta_2$  and  $\beta_3$  parameters were defined  
 333 based on the lapse rates computed at the seasonal time scale from observations. Ranges



334 for altitudinal thresholds  $z_1$  and  $z_2$  were deduced from other studies (Bookhagen and  
335 Burbank 2006, Nepal 2012, Savéan 2014). The initial ranges are given in TABLE 6.  
336 The size of parameter samples was chosen according to Sarrazin *et al.* (2016) (TABLE  
337 5) .

338 Maximum and minimum conditions on annual total precipitation for a set to be  
339 behavioral were chosen according to annual observed discharge for each of the two  
340 catchments. The mean observed discharge for the recorded period was 2043 mm/year  
341 at the Kharikhola station and 457 mm/year at the Tauche station. Annual total  
342 precipitation was expected to be greater than the measured annual discharge and  
343 lower than annual discharge plus 70%. These thresholds take into account both the  
344 uncertainty on measured discharges and actual evapotranspiration. Based no a values  
345 proposed in the literature, evapotranspiration is assumed to represent less than 50%  
346 of observed discharge, for both catchments. The minimum and maximum thresholds  
347 for both catchments are summarized TABLE 7.

348  
349 The method's convergence (i.e., the stability of the result when the sample size  
350 grows) was graphically assessed. The results converged for sample sizes from 1000  
351 samples. FIGURE 5 shows the cumulative density function (CDF) for behavioral  
352 and nonbehavioral parameter sets for the monsoon and winter seasons. Of the  
353 2000 parameter sets sampled, 712 sets verified the chosen minimum and maximum  
354 conditions for annual total precipitation and snowfall (i.e., they were behavioral). The  
355 sensitivity of the output to each parameter was evaluated by the maximum vertical  
356 distance (MVD) between CDF for behavioral and nonbehavioral parameter sets.  
357 Annual total precipitation appeared to be less sensitive to parameters controlling  
358 winter precipitation than to parameters controlling monsoon precipitation. This  
359 result can be explained by the fact that winter precipitation was less than monsoon  
360 precipitation. However, since the applied sampling method does not take into account  
361 the existing interaction between the five parameters, further analysis for parameter  
362 ranking was not significant.

363  
364 The method was necessarily sensitive to the prior hypothesis presented TABLE 5.  
365 In particular, the conditions for a set to be behavioral have a significant impact on the  
366 distribution of the behavioral sets. On the contrary, increasing the sample size does  
367 not affect the output distribution, since minimum size for convergence is reached.

**Table 5.** The algorithm selected, sample size and prior distribution for sampling the parameter space using the SAFE(R) toolbox (Pianosi *et al.* 2015).

Sample size	2000
Nb. of model evaluation	2000
Sampling algorithm	All-at-a-Time
Sampling method	Latin Hypercube
Prior distributions	Uniforms



**Table 6.** Initial ranges considered for the five shape parameters of the altitudinal factor:  $z_1$ ,  $z_2$ ,  $\beta_1$ ,  $\beta_2$  and  $\beta_3$ . Ranges are defined based on measurements at stations and on values founded in the literature.

	Minimum	Maximum	
$z_1$	1900	3500	m. a.s.l.
$z_2$	3500	6500	m. a.s.l.
$\beta_1$	0.00	2.00	$km^{-1}$
$\beta_2$	-2.00	0.00	$km^{-1}$
$\beta_3$	-0.30	0.00	$km^{-1}$

**Table 7.** Conditions over total precipitation on the Kharikhola and Tauche catchments for a parameter set to be behavioral. Annual total precipitation was expected to be greater than the measured annual discharge plus 20% and lower than annual discharge plus 50%.

	Minimum	Maximum	
Kharikhola	2043	3473	mm/year
Tauche	457	777	mm/year

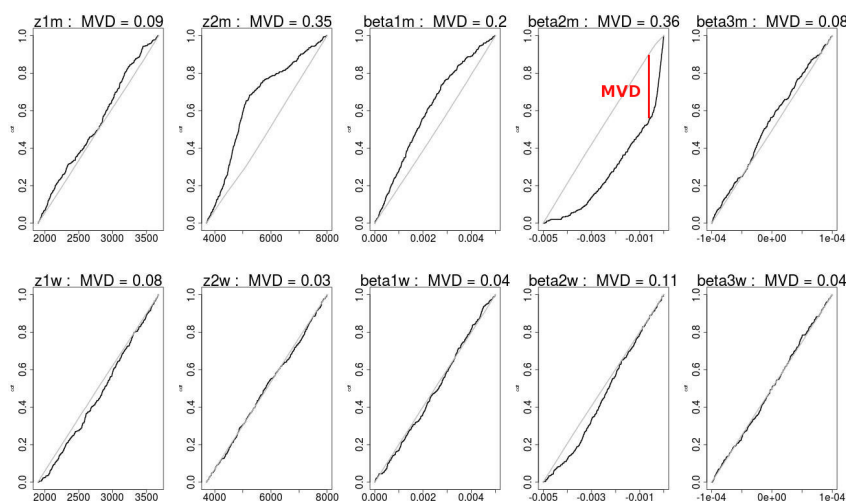


**Figure 5.** Cumulative density function of behavioral and non-behavioral output for each parameter for the two seasons. Black lines are cumulative distributions of behavioral parameter sets, and grey lines are cumulative distributions of non-behavioral sets. Parameters with indication w (respectively, m) stand for winter values (respectively, monsoon values). The greater the maximum vertical distance (MVD), the more influential the parameter was. MVD is drawn as an example for parameter beta2m.

## 368 5.2. Uncertainties analysis

### 369 5.2.1. Annual simulated water budgets

370 The precipitation fields generated using each behavioral parameter set were used as  
 371 input data within the ISBA surface scheme. The simulation over the Tauche and  
 372 Kharikhola catchments were run separately over the 2013-01-01/2016-03-31 period, at  
 373 the hourly time scale. The 2013–2014 year was used as a spin-up period and the results  
 374 were observed for 2014–2015 and 2015–2016 hydrological years. To overcome the issue



**Table 8.** Mean values ( $\bar{X}$ ), standard deviation ( $\sigma$ ) and relative standard deviation ( $\sigma/\bar{X}$ ) for total precipitation (PTOT), snowfall (SNOWF), discharge (RUNOFF) and actual evapotranspiration (EVAP) simulated with ISBA for the Kharikhola catchment or Tauche catchment: the mean for 2014–2015 and 2015–2016.

	Kharikhola catchment						Tauche catchment					
	2014-2015			2015-2016			2014-2015			2015-2016		
	$\bar{X}$	$\sigma$	$\sigma/\bar{X}$	$\bar{X}$	$\sigma$	$\sigma/\bar{X}$	$\bar{X}$	$\sigma$	$\sigma/\bar{X}$	$\bar{X}$	$\sigma$	$\sigma/\bar{X}$
	mm	mm	-	mm	mm	-	mm	mm	-	mm	mm	-
EVAP	604	17	3%	664	16	2%	213	16	8%	219	15	7%
PTOT	2868	295	10%	2069	207	10%	766	110	14%	525	82	16%
RUNOFF	2279	293	13%	1421	203	14%	517	128	25%	459	85	19%
SNOWF	32	8	25%	22	7	32%	364	56	15%	205	35	17%

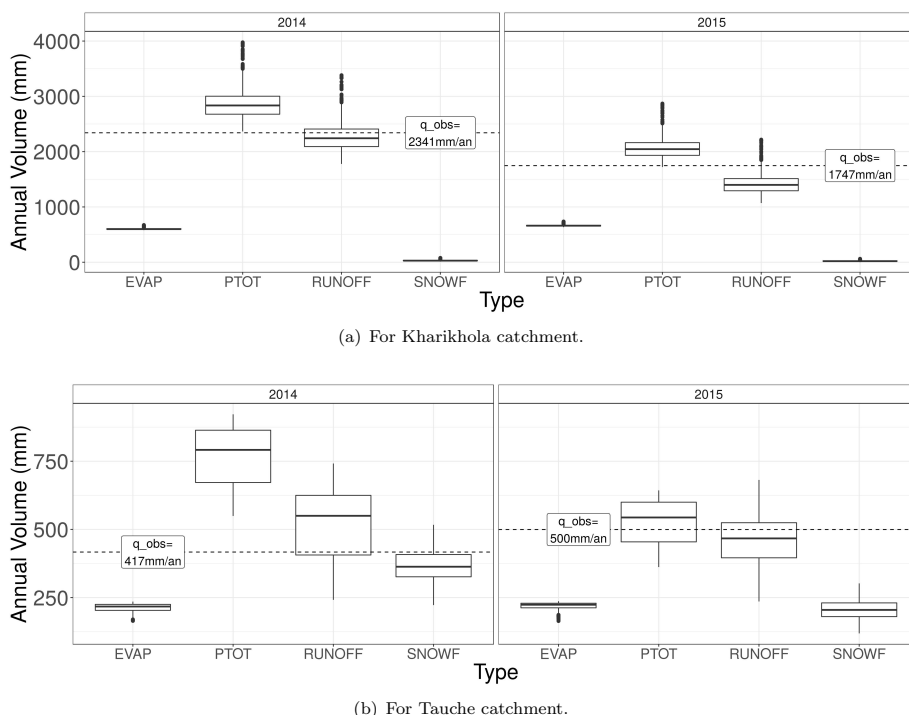
of calibrating a flow-routing module, the simulated discharge were aggregated at the annual time scale and compared to annual observed discharge at the outlet ( $\bar{Q}_{obs}$ ).

FIGURE 6 presents boxplots obtained for the 712 behavioral parameter sets for the terms of the annual water budget, i.e., liquid and solid precipitation, discharge and evapotranspiration. The dotted line represents  $\bar{Q}_{obs}$  for each catchment. The mean annual volumes of simulated variables were also computed for each parameter set in 2014–2015 and 2015–2016, and the intervals of uncertainty associated with simulated annual volumes are provided. This method highlights the propagation of uncertainties associated with the representation of orographic effects toward simulated terms of annual water budgets.

TABLE 8 presents the mean value, standard deviation and relative standard deviation for all of the ISBA simulated variables for the Kharikhola and Tauche catchments, for 2014–2015 and 2015–2016. The annual actual evapotranspiration accounted for 26% of annual total precipitation for Kharikhola and 34% for Tauche. In comparison, evapotranspiration was estimated at about 20%, 14% and 53% of total annual precipitation, respectively, by (Andermann *et al.* 2012), (Nepal *et al.* 2014) and (Savéan *et al.* 2015) over the entire Dudh Koshi basin and (Ragettli *et al.* 2015) estimated it at 36.2% of annual total precipitation for the upper part of the Langtang basin.

Annual snow fall volume for Kharikhola was a neglectible fraction of annual total precipitation ( $\sim 1\%$ ) and it was around 44% for Tauche. Annual snowfall was estimated at, respectively, 15.6% and 51.4% of annual total precipitation by (Savéan *et al.* 2015) (entire Dudh Koshi river basin) and (Ragettli *et al.* 2015) (upper part of the Langtang basin).

Moreover, this statistical approach shows that the only uncertainties associated with representation of the orographic effect results in significant uncertainties on simulated variables. These uncertainties account for up to 16% for annual total precipitation, up to 25% for annual discharge and up to 8% for annual actual evapotranspiration. Uncertainty on annual snowfall is quantified at 16% for high mountain catchment and up to 32% for middle mountain catchment. These uncertainty intervals are essentially conditioned by model structure and parametrization, and these results point out that simulated water budgets provided by modelling studies must necessarily be associated with error intervals.



**Figure 6.** Boxplots for distribution of annual volumes of the terms of the water budget: Discharge (RUNOFF), solid and total precipitation (SNOWF and PTOT) and evapotranspiration (EVAP) for 2014–2015, for the Kharikhola and Tauche catchments.

411 5.2.2. Toward optimizing parameter sets with bias on annual discharge

412 Going further into the simulation results, the hydrological cycle was inverted, in order  
 413 to use observed discharge to optimize the relation between precipitation and altitude,  
 414 as presented for mountainous areas by Valéry *et al.* (2009). Precipitation fields were  
 415 then constrained at the local scale according to simulated discharges. Annual bias  
 416 on discharge were computed for each catchment as the absolute value of the ratio  
 417 between the observed and simulated annual discharges minus 1. FIGURE 7 presents  
 418 the scatter plot of the distributions of bias on annual discharge for the Kharikhola  
 419 and Tauche catchments. The Pareto optimums minimizing bias on annual discharge  
 420 for both catchments were computed using the R rPref package (Rocks and Rocks  
 421 2016). For exemple, the ten first Pareto optimums were selected among the 712 behav-  
 422 ioral parameter sets considered. The values of parameters for the winter and monsoon  
 423 seasons for the ten first optimum sets are summarized in TABLE 9. For the ten param-  
 424 eter sets selected, the altitudinal threshold z1 was located between 2010 m.a.s.l. and  
 425 3470 m.a.s.l. during the monsoon season and between 2287 m.a.s.l. and 3488 m.a.s.l.  
 426 during winter. The second altitudinal threshold z2 was located between 3709 m.a.s.l.  
 427 and 6167 m.a.s.l. during monsoon and between 3734 m.a.s.l. and 6466 m.a.s.l. during  
 428 winter. Altitudes found for z1 were globally higher than altitudes proposed in the liter-  
 429 ature for the second mode of precipitation (between 1800 m.a.s.l. and 2400 m.a.s.l.,



430 as described in section 3.2.2). Since these values were calibrated at the local scale, ac-  
 431 cording to ground-based measurements, they can be considered to accurately represent  
 432 the local variability encountered in the Tauche and Kharikhola catchments. Moreover,  
 433 values for an altitudinal threshold of precipitation located above 4000 m.a.s.l. were  
 434 proposed.

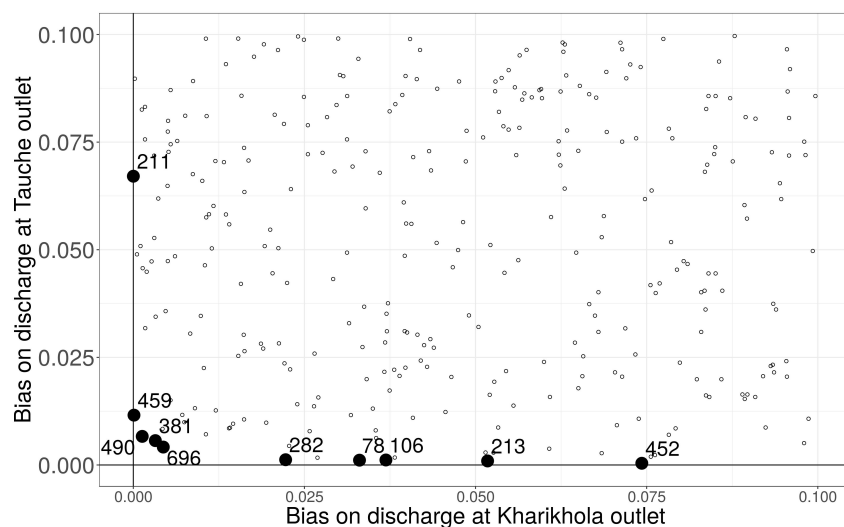


**Figure 7.** Scatter plot of bias on mean annual discharges for the Kharikhola and Tauche catchments for 2014–2015. Darker dots are parameter sets that provide the ten first Pareto optimums according to both criteria: bias for discharges on the Kharikhola and Tauche catchments. Optimal value for bias is 0. Graphical window is limited.

**Table 9.** Values of parameters for the winter and monsoon seasons for the ten first Pareto optimum sets. The Pareto optimums minimize bias on annual discharge for both catchments.

Sample $n^\circ$	78	106	211	213	282	381	452	459	490	696	
z1m	3470	3066	3286	2010	2971	2946	3337	2333	2064	2253	m.a.s.l.
z2m	3709	4938	6101	4379	4813	5596	5681	3915	6167	5978	m.a.s.l.
beta1m	0.032	0.028	0.455	1.772	1.089	1.755	0.787	0.73	0.135	0.003	$km^{-1}$
beta2m	-1.382	-0.48	-0.556	-0.143	-0.169	-0.397	-0.516	-1.394	-0.587	-0.341	$km^{-1}$
beta3m	-0.283	-0.229	-0.059	-0.207	-0.298	-0.037	-0.003	-0.25	-0.033	-0.111	$km^{-1}$
z1w	3113	2727	2287	2895	3236	2623	2446	3488	2554	2639	m.a.s.l.
z2w	4943	4716	3871	6466	5657	3734	4336	5163	4732	5155	m.a.s.l.
beta1w	1.917	0.288	0.869	1.533	1.658	0.293	0.115	1.729	1.256	0.348	$km^{-1}$
beta2w	-1.83	-1.096	-1.588	-1.791	-0.804	-0.455	-1.568	-1.457	-1.612	-0.508	$km^{-1}$
beta3w	-0.191	-0.2	-0.255	-0.244	-0.068	-0.165	-0.294	-0.011	-0.039	-0.037	$km^{-1}$
bias Khari.	0.033	0.037	0	0.052	0.022	0.003	0.074	0	0.001	0.004	
bias Tauche	0.001	0.001	0.067	0.001	0.001	0.006	0	0.012	0.007	0.004	



435 *5.2.3. Ensemble of hourly precipitation fields on the Dudh Koshi River basin*

436 Observed precipitation at measuring stations were then interpolated at the hourly time  
437 scale over the Dudh Koshi River basin at the 1-km spatial resolution. The method  
438 given by EQUATION 2 is applied, using shape parameters for the altitudinal factor  
439 selected TABLE 9. The average annual volumes of computed total precipitation ranged  
440 between 1365 mm and 1652 mm, and annual snowfall volumes ranged between 89 mm  
441 and 126 mm, in average over the 2014–2015 and 2015–2016 hydrological years. These  
442 values are consistent with other products available for the area. In particular, Savéan  
443 (2014) showed that the APHRODITE (Yatagai *et al.* 2012) product underestimates  
444 total precipitation over the Dudh Koshi River basin, with annual total precipitation of  
445 1311 mm for the interannual average between 2001 and 2007, and Nepal *et al.* (2014)  
446 proposed a mean annual total precipitation for the Dudh Koshi basin of 2114 mm  
447 over the 1986–1997 period. The ERA-Interim reanalysis (25-km resolution) provided a  
448 mean annual precipitation of 1743 mm over the 2000–2013 period. Different relations  
449 between altitude and annual precipitation are then represented. The higher (lower)  
450 values are the positive (negative) rates, the sharpest are the spatial variations of annual  
451 precipitation. This has to be discussed considering the physical properties of convection  
452 at such high altitudes.

453 **6. Conclusion**

454 The main objective of this paper was to provide a representation of the effect of alti-  
455 tude on precipitation that represent spatial and temporal variability of precipitation  
456 in the Everest region. A weighted inverse distance method coupled with a multiplica-  
457 tive altitudinal factor was applied to spatially extrapolate measured precipitation  
458 for the Dudh Koshi basin is shown to acceptably fit a piecewise linear function of  
459 altitude, with significant seasonal variations. A sensitivity analysis was run to reduce  
460 the variation interval for parameters controlling the shape of the altitudinal factor.  
461 An uncertainty analysis was subsequently run to evaluated ensemble of simulated  
462 variables according to observed discharge for two small subcatchments of the Dudh  
463 Koshi basin located in mid- and high-altitude mountain environments.  
464

465 Non deterministic annual water budgets are provided for two small gauged  
466 subcatchments located in high- and mid-altitude mountain environments. This work  
467 shows that the only uncertainties associated with representation of the orographic ef-  
468 fect account for about 16% for annual total precipitation and up to 25% for simulated  
469 discharges. Annual evapotranspiration is shown to represent  $26\% \pm 1\%$  of annual  
470 total precipitation for the mid-altitude catchment and  $34\% \pm 3\%$  for the high-altitude  
471 catchment. Snow fall contribution is shown to be neglectible for the mid-altitude  
472 catchment and it represents up to  $44\% \pm 8\%$  of total precipitation for the high-altitude  
473 catchment. These simulations at the local scale enhance current knowledge of the  
474 spatial variability of hydro-climatic processes in high- and mid-altitude mountain  
475 environments.  
476

477  
478 This work paves the way to produce hourly precipitation maps extrapolated from  
479 ground-based measurements that are reliable at the local scale. However, additional  
480 criteria would be needed to provide a single optimum parameter set for altitudinal



481 factor that would be suitable for the entire Dudh Koshi River basin. For example, snow  
482 cover areas simulated at a scale larger than the two catchments could be compared  
483 to available remote products (Behrangi *et al.* 2016). Independent measurements of  
484 precipitation could also be used to constrain the ensemble of precipitation fields.

485  
486 Moreover, since observations are made over a very short duration and contain long  
487 periods with missing information, the results are limited to the 2014–2015 and 2015–  
488 2016 hydrological years and to the Dudh Koshi River basin. In addition, this study  
489 focuses only on one source of uncertainty in the measurement-spatialization-modeling  
490 chain, whereas sensitivity analysis should include all types of uncertainty (Beven 2015,  
491 Saltelli *et al.* 2006). A more complete method would include epistemic uncertainty  
492 on model parameters and aleatory uncertainty on input variables in the sensitivity  
493 analysis (Fuentes Andino *et al.* 2016).

#### 494 Acknowledgements

495 The authors extend special thanks to Professor Isabelle Sacareau (Passages Labora-  
496 tory of the CNRS and Montaigne University of Bordeaux, France), coordinator of the  
497 Preshine Project. They are also grateful to the hydrometry team and the administra-  
498 tive staff of the Laboratoire Hydrosociences Montpellier, France, the hydrologists of the  
499 Institut des Geosciences de l'Environnement in Grenoble, France, the meteorologists of  
500 the Centre National de la Recherche Meteorologique in Toulouse and Grenoble, France,  
501 the Association Ev-K2 CNR and the Pyramid Laboratory staff in Bergamo, Italy,  
502 Kathmandu and Lobuche, Nepal, and the Vice-Chancellor of the Nepalese Academy  
503 of Science and Technology. The authors are particularly grateful to Professor Keith  
504 Beven from Lancaster University (UK) and to Dr. Patrick Wagnon from Institut de  
505 Recherche pour le Developpement. Finally, they pay homage to the local observers,  
506 local authorities, Sagarmatha National Park and the Cho-Oyu trekking agency with  
507 its respective staff and porters.

#### 508 Funding

509 This work was funded by the Agence Nationale de la Recherche (references ANR-  
510 09-CEP-0005-04/PAPRIKA and ANR-13-SENV-0005-03/PRESHINE), Paris, France.  
511 It was locally approved by the Bilateral Technical Committee of the Ev-K2-CNR  
512 Association (Italy) and the Nepal Academy of Science and Technology (NAST) within  
513 the Ev-K2-CNR/NAST Joint Research Project. It is supported by the Department of  
514 Hydrology and Meteorology, Kathmandu, Nepal.

#### 515 References

- 516 Alpert, P., 1986. Mesoscale indexing of the distribution of orographic precipitation over high  
517 mountains. *Journal of climate and applied meteorology*, 25 (4), 532–545.  
518 Andermann, C., *et al.*, 2012. Impact of transient groundwater storage on the discharge of  
519 himalayan rivers. *Nature Geoscience*, 5 (2), 127–132.  
520 Andermann, C., Bonnet, S., and Gloaguen, R., 2011. Evaluation of precipitation data sets  
521 along the himalayan front. *Geochemistry, Geophysics, Geosystems*, 12 (7).



- 522 Anders, A.M., *et al.*, 2006. Spatial patterns of precipitation and topography in the himalaya.  
523 *Geological Society of America Special Papers*, 398, 39–53.
- 524 Arino, O., *et al.*, 2012. Global land cover map for 2009 (globcover 2009).
- 525 Barros, A.P. and Lettenmaier, D.P., 1993. Dynamic modeling of the spatial distribution of  
526 precipitation in remote mountainous areas. *Monthly weather review*, 121 (4), 1195–1214.
- 527 Barros, A., *et al.*, 2000. A study of the 1999 monsoon rainfall in a mountainous region in central  
528 nepal using trmm products and rain gauge observations. *Geophysical Research Letters*, 27  
529 (22), 3683–3686.
- 530 Barros, A., *et al.*, 2004. Probing orographic controls in the himalayas during the monsoon  
531 using satellite imagery. *Natural Hazards and Earth System Science*, 4 (1), 29–51.
- 532 Behrangī, A., *et al.*, 2016. Using grace to constrain precipitation amount over cold mountainous  
533 basins. *Geophysical Research Letters*.
- 534 Bénichou, P. and Le Breton, O., 1987. AURELHY : une méthode d'analyse utilisant le  
535 relief pour les besoins de l'hydrométéorologie. In: *Deuxièmes journées hydrologiques de*  
536 *l'ORSTOM à Montpellier. Colloques et Séminaires. ORSTOM*, 299–304. Available from:  
537 <http://www.documentation.ird.fr/hor/fdi:25973>.
- 538 Beven, K., 2010. *Environmental modelling: An uncertain future?* CRC Press.
- 539 Beven, K., 2015. Facets of uncertainty: epistemic uncertainty, non-stationarity, likelihood, hy-  
540 pothesis testing, and communication. *Hydrological Sciences Journal*, (just-accepted).
- 541 Bharati, L., *et al.*, 2014. The Projected Impact of Climate Change on Water Availability  
542 and Development in the Koshi Basin, Nepal. *Mountain Research and Development*, 34 (2),  
543 118–130. Available from: [http://www.bioone.org/doi/abs/10.1659/MRD-JOURNAL-D-13-](http://www.bioone.org/doi/abs/10.1659/MRD-JOURNAL-D-13-00096.1)  
544 [00096.1](http://www.bioone.org/doi/abs/10.1659/MRD-JOURNAL-D-13-00096.1).
- 545 Bharati, L., *et al.*, 2016. Past and future variability in the hydrological regime of the koshi  
546 basin, nepal. *Hydrological Sciences Journal*, 61 (1), 79–93.
- 547 Bookhagen, B. and Burbank, D.W., 2006. Topography, relief, and trmm-derived rainfall  
548 variations along the himalaya. *Geophysical Research Letters*, 33 (8). Available from:  
549 <http://dx.doi.org/10.1029/2006GL026037>.
- 550 Bookhagen, B. and Burbank, D.W., 2010. Toward a complete Himalayan hydrological budget:  
551 Spatiotemporal distribution of snowmelt and rainfall and their impact on river discharge.  
552 *Journal of geophysical research-Earth surface*, 115.
- 553 Boone, A., *et al.*, 2000. The influence of the inclusion of soil freezing on simulations by a  
554 soil-vegetation-atmosphere transfer scheme. *JOURNAL OF APPLIED METEOROLOGY*,  
555 39 (9), 1544–1569.
- 556 Boone, A. and Etchevers, P., 2001. An intercomparison of three snow schemes of varying com-  
557 plexity coupled to the same land surface model: Local-scale evaluation at an alpine site. *Jour-*  
558 *nal of Hydrometeorology*, 2 (4), 374–394. Available from: [http://dx.doi.org/10.1175/1525-](http://dx.doi.org/10.1175/1525-7541(2001)002j0374:A10TSSj2.0.CO;2)  
559 [7541\(2001\)002j0374:A10TSSj2.0.CO;2](http://dx.doi.org/10.1175/1525-7541(2001)002j0374:A10TSSj2.0.CO;2).
- 560 Burns, J.I., 1953. Small-scale topographic effects on precipitation distribution in san dimas  
561 experimental forest. *Eos, Transactions American Geophysical Union*, 34 (5), 761–768.
- 562 Chapman, T., 1999. A comparison of algorithms for stream flow recession and  
563 baseflow separation. *Hydrological Processes*, 13 (5), 701–714. Available from:  
564 [http://dx.doi.org/10.1002/\(SICI\)1099-1085\(19990415\)13:5j701::AID-HYP774j3.0.CO;2-2](http://dx.doi.org/10.1002/(SICI)1099-1085(19990415)13:5j701::AID-HYP774j3.0.CO;2-2).
- 565 Congedo, L., 2015. Semi-automatic classification plugin documentation. *Release*, 4 (0.1), 29.
- 566 Cosgrove, B., *et al.*, 2003. Real-time and retrospective forcing in the North American  
567 Land Data Assimilation System (NLDAS) project. *JOURNAL OF GEOPHYSICAL*  
568 *RESEARCH-ATMOSPHERES*, 108 (D22).
- 569 Daly, C., *et al.*, 2002. A knowledge-based approach to the statistical mapping of climate.  
570 *Climate research*, 22 (2), 99–113.
- 571 Decharme, B., *et al.*, 2011. Local evaluation of the Interaction between Soil Biosphere Atmo-  
572 sphere soil multilayer diffusion scheme using four pedotransfer functions. *JOURNAL OF*  
573 *GEOPHYSICAL RESEARCH-ATMOSPHERES*, 116.
- 574 Dhar, O. and Rakhecha, P., 1981. The effect of elevation on monsoon rainfall distribution in  
575 the central himalayas. *Monsoon Dynamics*, 253–260.



- 576 Drusch, M., *et al.*, 2012. Sentinel-2: Esa's optical high-resolution mission for gmes operational  
577 services. *Remote Sensing of Environment*, 120, 25–36.
- 578 Dümenil, L. and Todini, E., 1992. A rainfall-runoff scheme for use in the hamburg climate  
579 model. In: *Advances in theoretical hydrology: a tribute to james dooge*. Elsevier Science  
580 Publishers BV, 129–157.
- 581 Frei, C. and Schär, C., 1998. A precipitation climatology of the alps from high-resolution  
582 rain-gauge observations. *International Journal of climatology*, 18 (8), 873–900.
- 583 Fuentes Andino, D., *et al.*, 2016. Event and model dependent rainfall adjustments to improve  
584 discharge predictions. *Hydrological Sciences Journal*, (just-accepted).
- 585 Gongsa-Saholiariliva, N., *et al.*, 2016. Geostatistical estimation of daily monsoon precipitation  
586 at fine spatial scale: Koshi river basin. *Journal of Hydrologic Engineering*, 05016017.
- 587 Gottardi, F., *et al.*, 2012. Statistical reanalysis of precipitation fields based on ground network  
588 data and weather patterns: Application over french mountains. *Journal of Hydrology*, 432,  
589 154–167.
- 590 Hagemann, S., 2002. *An improved land surface parameter dataset for global and regional climate*  
591 *models*. Max-Planck-Institut für Meteorologie.
- 592 Heynen, M., *et al.*, 2016. Air temperature variability in a high-elevation himalayan catchment.  
593 *Annals of Glaciology*, 57 (71), 212–222.
- 594 Immerzeel, W.W., *et al.*, 2012. Hydrological response to climate change in a glacierized catch-  
595 ment in the Himalayas. *Climatic change*, 110 (3-4), 721–736.
- 596 Immerzeel, W., *et al.*, 2014. The importance of observed gradients of air temperature and  
597 precipitation for modeling runoff from a glacierized watershed in the nepalese himalayas.  
598 *Water Resources Research*, 50 (3), 2212–2226.
- 599 Kansakar, S.R., *et al.*, 2004. Spatial pattern in the precipitation regime of nepal. *International*  
600 *Journal of Climatology*, 24 (13), 1645–1659.
- 601 Koeppe, C.E. and De Long, G., 1958. Weather and climate.
- 602 Koffler, D. and Laaha, G., 2013. Lfstat-low-flow analysis in r. In: *EGU General Assembly*  
603 *Conference Abstracts*. vol. 15, 7770.
- 604 Lang, M., *et al.*, 2006. Incertitudes sur les débits de crue. *La Houille Blanche-Revue interna-*  
605 *tionale de l'eau*, 6, p–33.
- 606 Lang, T.J. and Barros, A.P., 2004. Winter storms in the central himalayas. *Journal of Meteoro-*  
607 *logical Society of Japan*, 82 (3), 829–844.
- 608 Masson, V., *et al.*, 2003. A global database of land surface parameters at 1-km resolution in  
609 meteorological and climate models. *Journal of climate*, 16 (9), 1261–1282.
- 610 Nepal, S., *et al.*, 2014. Understanding the hydrological system dynamics of a glaciated alpine  
611 catchment in the Himalayan region using the J2000 hydrological model. *Hydrological Pro-*  
612 *cesses*, 28 (3), 1329–1344.
- 613 Nepal, S., 2012. *Evaluating upstream-downstream linkages of hydrological dynamics in the hi-*  
614 *malayan region*. Thesis (PhD). PhD Thesis. Friedrich Schiller University, Germany.
- 615 Nepal, S., Flügel, W.A., and Shrestha, A.B., 2014. Upstream-downstream linkages of hydro-  
616 logical processes in the himalayan region. *Ecological Processes*, 3 (1), 1.
- 617 Noilhan, J. and Mahfouf, J.F., 1996. The isba land surface parameterisation scheme. *Global*  
618 *and planetary Change*, 13 (1), 145–159.
- 619 Noilhan, J. and Planton, S., 1989. A Simple Parameterization of Land Surface Processes  
620 for Meteorological Models. *Monthly Weather Review*, 117 (3), 536–549. Available from:  
621 [http://dx.doi.org/10.1175/1520-0493\(1989\)117<0536:ASPOLS>2.0.CO;2](http://dx.doi.org/10.1175/1520-0493(1989)117<0536:ASPOLS>2.0.CO;2).
- 622 Pellicciotti, F., *et al.*, 2012. Challenges and uncertainties in hydrological modeling of remote  
623 hindu kush-karakoram-himalayan (hkh) basins: suggestions for calibration strategies. *Moun-*  
624 *tain Research and Development*, 32 (1), 39–50.
- 625 Pianosi, F., Sarrazin, F., and Wagener, T., 2015. A matlab toolbox for global sen-  
626 sitivity analysis. *Environmental Modelling & Software*, 70, 80 – 85. Available from:  
627 <http://www.sciencedirect.com/science/article/pii/S1364815215001188>.
- 628 Pokhrel, B.K., *et al.*, 2014. Comparison of two snowmelt modelling approaches in the dudh  
629 koshi basin (eastern himalayas, nepal). *Hydrological Sciences Journal*, 59 (8), 1507–1518.



- 630 Ragettli, S., *et al.*, 2015. Unraveling the hydrology of a himalayan catchment through  
631 integration of high resolution in situ data and remote sensing with an ad-  
632 vanced simulation model. *Advances in Water Resources*, 78, 94–111. Available from:  
633 <http://linkinghub.elsevier.com/retrieve/pii/S0309170815000159>.
- 634 Roe, G.H., 2005. Orographic precipitation. *Annu. Rev. Earth Planet. Sci.*, 33, 645–671.
- 635 Roocks, P. and Roocks, M.P., 2016. Package rpref.
- 636 Salerno, F., *et al.*, 2015. Weak precipitation, warm winters and springs impact glaciers of south  
637 slopes of mt. everest (central himalaya) in the last 2 decades (1994–2013). *The Cryosphere*,  
638 9 (3), 1229–1247.
- 639 Saltelli, A., *et al.*, 2006. Sensitivity analysis practices: Strategies for model-based inference.  
640 *Reliability Engineering & System Safety*, 91 (10), 1109–1125.
- 641 Sarrazin, F., Pianosi, F., and Wagener, T., 2016. Global sensitivity analysis of environmental  
642 models: Convergence and validation. *Environmental Modelling & Software*, 79, 135 – 152.  
643 Available from: <http://www.sciencedirect.com/science/article/pii/S1364815216300251>.
- 644 Savéan, M., 2014. *Modélisation hydrologique distribuée et perception de la variabilité hydro-*  
645 *climatique par la population du bassin versant de la dudh koshi (népal)*. Thesis (PhD).  
646 Université de Montpellier 2.
- 647 Savéan, M., *et al.*, 2015. Water budget on the Dudh Koshi River (Nepal):  
648 Uncertainties on precipitation. *Journal of Hydrology*. Available from:  
649 <http://linkinghub.elsevier.com/retrieve/pii/S0022169415008082>.
- 650 Sevruk, B., Ondrás, M., and Chvíla, B., 2009. The wmo precipitation measurement intercom-  
651 parisons. *Atmospheric Research*, 92 (3), 376–380.
- 652 Shrestha, D., Singh, P., and Nakamura, K., 2012. Spatiotemporal variation of rainfall over  
653 the central himalayan region revealed by trmm precipitation radar. *Journal of Geophysical*  
654 *Research: Atmospheres*, 117 (D22).
- 655 Spear, R. and Hornberger, G., 1980. Eutrophication in peel inletii. identification of critical  
656 uncertainties via generalized sensitivity analysis. *Water Research*, 14 (1), 43 – 49. Available  
657 from: <http://www.sciencedirect.com/science/article/pii/0043135480900408>.
- 658 Valéry, A., Andréassian, V., and Perrin, C., 2009. Inverting the hydrological cy-  
659 cle: when streamflow measurements help assess altitudinal precipitation gradi-  
660 ents in mountain areas. *New approaches to hydrological prediction in data sparse*  
661 *regions*. Wallingford: IAHS Press, IAHS Publ, 333, 281–286. Available from:  
662 <http://hydrologie.org/redbooks/a333/IAHS3330281.pdf>.
- 663 Valéry, A., Andréassian, V., and Perrin, C., 2010. Regionalization of precipitation and air  
664 temperature over high-altitude catchments learning from outliers. *Hydrological Sciences*  
665 *Journal*, 55 (6), 928–940. Available from: <http://dx.doi.org/10.1080/02626667.2010.504676>.
- 666 World Meteorological Organization, 2008. *Manual on low-flow estimation and prediction*.  
667 Geneva, Switzerland: World Meteorological Organization.
- 668 Yatagai, A., *et al.*, 2012. Aphrodite: Constructing a long-term daily gridded precipitation  
669 dataset for asia based on a dense network of rain gauges. *Bulletin of the American Mete-*  
670 *orological Society*, 93 (9), 1401–1415.